Available online at www.sciencedirect.com
ScienceDirect
Journal of Sound and Vibration 324 (2009) 712–732
JOURNAL OF SOUND AND VIBRATION
www.elsevier.com/locate/jsvi

Numerical and experimental investigation of the effect of structural links on the sound transmission of a lightweight double panel structure

Julien Legault*, Noureddine Atalla

GAUS, Department of Mechanical Engineering, Université de Sherbrooke, Sherbrooke, Quebec, Canada J1K 2R1

Received 12 November 2008; received in revised form 17 February 2009; accepted 18 February 2009
Handling Editor: C.L. Morfey

Abstract

This paper examines various models predicting the influence of periodically spaced structural links on sound transmission through lightweight double panel structures. A baseline configuration made up from two aluminum plates connected through aluminum C-section channels and a fiberglass filled cavity has been specifically built and its TL measured for comparison and validation of the investigated models. First, classical decoupled approaches are outlined and adapted for the studied case. Next, a periodic model based on existing formulations is presented. The model allows for a 3D incident field and accounts for the absorption in the cavity with the help of an equivalent fluid model for the fiberglass. Three cases of coupling conditions are considered for the links: a mass–spring–mass approximation, a beam-type approximation and a beam-type approximation where the rigidity and the inertia of the beams are neglected. The measurements show that the bridged configuration strongly reduces the TL at mid and high frequency and exhibits pass/stop bands characteristic of periodic structures. The predictions of decoupled approaches capture the physics of the problem only approximately and with the integration of the mass of the connectors in the context of thin lightweight panels, their agreement with experimental data is further reduced. On the other hand, the results obtained with the periodic model are excellent over most of the studied frequency range. However, in the vicinity of the critical frequency of the thicker panel (around 6 kHz), an overestimation of the TL is observed. This suggests that the model will have to account better for damping and resonant transmission.

1. Introduction

Double panel structures filled with air or absorbent fiberglass can be found in a wide range of applications and were therefore extensively studied in the literature. A recent article by Hongisto [1] provided a detailed comparison of the prevalent models for the prediction of sound transmission through such constructions. Over the 20 models presented, only a few were able to deal with connections between the panels: Sharp [2,3], Gu and Wang [4], Fahy [5] and Davy [6,7]. In these four models, the problem was addressed by decoupling the

*Corresponding author. Tel.: +1 819 821 8000x62122.
E-mail address: julien.legault@usherbrooke.ca (J. Legault).

0022-460X/$ - see front matter © 2009 Elsevier Ltd. All rights reserved.
doi:10.1016/j.jsv.2009.02.019

total transmission in terms of a fluid-borne path through the cavity and a structure-borne path through the connectors. They will be referred here as ''decoupled approaches''.

Yet, many other types of formulations were developed to include the effect of structural links. Among them, approaches taking advantage of the periodicity of the structure were presented by several authors. In the latter, the equations of motion of the plates include the reactions of the connectors in addition to the pressures due to fluid loading. To solve the associated systems, two methods are classically used. The first method was introduced by Mead and Pujara [8,9] and consists of representing the response of the structure in terms of a series of space-harmonics. The principle of virtual work is then applied on one period of the system to solve its dynamics. Lee and Kim [10] employed this technique to study the radiation of a single stiffened plate subjected to a plane wave excitation. Wang et al. [11] extended the approach to double-leaf partitions connected through vertical resilient studs. Urusovskii [12] had previously studied the problem using space-harmonic series to represent the plates' response, but he assumed rigid studs and did not use the principle of virtual work to formulate the dynamics. Instead, he introduced the ''phase factor'' associated with the force exerted on the plates by the stud as a result of oblique incidence in the equations of motion. The second method makes use of Fourier transform techniques. This is the case of Lin and Garrelick [13] who calculated sound transmission through double-plate structures attached periodically by rigid connectors. To study radiation under mechanical excitation forces of point connected, point connected with rib stiffening and rib connected structures, Takahashi [14] used the Fourier transform as well, but his equations did not include fluid loading. Ultimately, even if the solving procedure behind the two approaches is not similar, both lead to solutions in which the response is given as a series of space harmonics [15].

When simulations or experimental validations were conducted in the above-mentioned references, attention was principally focused on building constructions which are typically composed of plasterboard panels connected with wooden studs or metallic channels. Although they are not strictly equivalent to these structures, lightweight aircraft sidewall panels are good examples of double panel partitions since they are frequently made of periodically rib-connected panels with fiberglass in-between. Moreover, the rivets attaching the ribs to the plates and/or the trim mounts are close-spaced to provide stiffness. In comparison, the distance between the screws or nails used to bond the plasterboard panels to the wooden/metallic skeleton in buildings is normally larger. Craik and Smith [16] discussed the fact that when this spacing is small, the connection can be modeled by a continuous line. However, when it gets larger, each point can be assumed independent and so the coupling may be modeled as a series of independent point connections. The appropriate transition frequency between these two regimes occurs when a half bending wave-length on the plate fits between the nails or the screws. Considering the above-mentioned differences, using experimental or simulations results of building partitions may not be adequate to validate the performance of classical prediction models for lightweight double wall systems with periodic connections. The aim of this paper is therefore to examine experimentally and numerically the effect of periodically spaced mechanical links on the transmission loss of a double panel structure that is more representative of aircraft applications.

First, the studied structure is described (geometry, dimensions, connection details, etc.). Next, the decoupled approaches [2–7] presented in Ref. [1] are outlined and adapted to the studied case. Afterwards, a periodic model integrating important features of previous models [8–14] is exploited and extended to account for the nature of the studied mechanical link and cavity absorption. This is done by using an equivalent fluid model for the fibrous material [17]. A result section in which the studied models are compared to measurements is finally presented. It is followed by a general discussion on the accuracy of the various prediction methods.

2. Preliminary considerations

2.1. The studied structure

Figs. 1 and 2 present the double wall system studied throughout this document. It is made up from two 1220 mm × 2030 mm aluminum plates (1 and 2 mm thick) separated by a 50.8 mm cavity filled with a fibrous material. The Biot acoustic properties of the material (porosity, flow resistivity, tortuosity and characteristic lengths) were measured at the Université de Sherbrooke's acoustic materials characterization lab using direct methods (anisotropy is neglected and only the properties in the through thickness direction were measured).

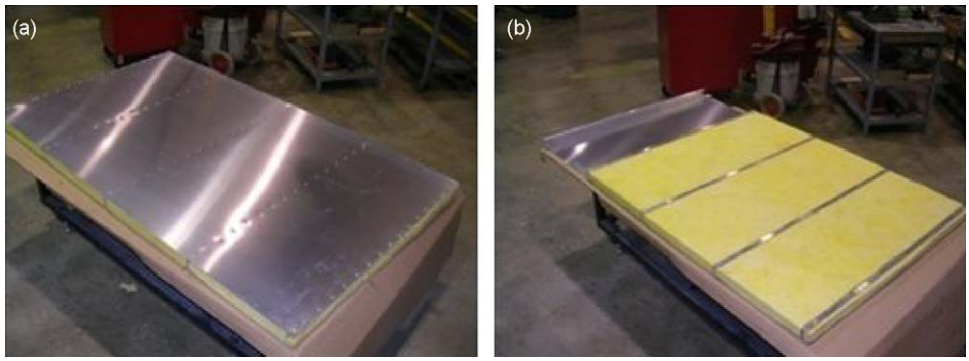

Fig. 1. The studied double wall structure: (a) complete structure, (b) first panel missing.

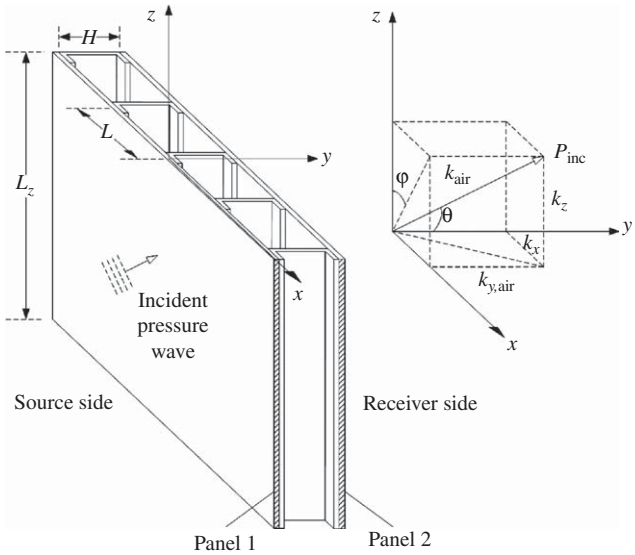

Fig. 2. Pressure wave impinging upon the double wall partition.

Table 1
Dynamic properties of the fibrous material (property, value).

Density of the fluid phase	$1.21\,\mathrm{kg\,m^{-3}}$
Speed of sound in the fluid phase	$342\,\mathrm{m\,s^{-1}}$
Flow resistivity	$17\,700\,\mathrm{N\,m\,s^{-4}}$
Porosity	0.91
Tortuosity	1.0
Viscous length	$128\times10^{-6}\,\mathrm{m}$
Thermal length	$376\times10^{-6}\,\mathrm{m}$
Density of the solid phase	$35.0\,\mathrm{kg\,m^{-3}}$

They are given in Table 1 and will be used in the equivalent fluid model of the material [17]. The aluminum panels are linked with five "C-section" channels (also in aluminum), each spaced by a distance L of 508 mm. The thickness e_B of the channels is 3.175 mm, while their web length H measures 50.8 mm and their flange length L_F measures 25.4 mm. They have a Young modulus E_B of $70\times10^9\,\mathrm{N\,m^{-2}}$, a Poisson's ratio ν_B of 0.33 and a density ρ_B of $2742\,\mathrm{kg\,m^{-3}}$. Using these geometrical and mechanical properties, equivalent section

Table 2
Properties of the C-section channels (property, symbol, value).

Mass per unit length	m'_B	$8.85 \times 10^{-1}\,\mathrm{kg\,m^{-1}}$
Second moment of area with respect to the x axial axis (see Fig. 2)	I_x	$1.39 \times 10^{-7}\,\mathrm{m^4}$
Distance between the section centroid and section shear center	c_x	$15.9 \times 10^{-3}\,\mathrm{m}$
Moment of inertia per unit length in the z direction with respect to centroidal axial axis	I_O	$1.76 \times 10^{-4}\,\mathrm{kg\,m}$
Moment of inertia per unit length in the z direction with respect to shear center axial axis	I_S	$3.98 \times 10^{-4}\,\mathrm{kg\,m}$
Torsional constant in the z direction	J_z	$1.21 \times 10^{-9}\,\mathrm{m^4}$
Torsion-bending section constant associated to warping	Γ	$9.79 \times 10^{-12}\,\mathrm{m^6}$

properties of the channels were computed with the help of text books formulas [18]. They are given in Table 2. To attach the channels to the panels, 76.2 mm spaced screws were used. The holes were threaded and nuts were employed to tighten the assembly. However, the exact torque was not measured. In addition, a layer of silicone was used between the surface of the channels and the panels to approximate a full line coupling condition, i.e. to reduce the impact of discrete screw spacing.

It is certain that with such attributes, the studied structure does not render all the complexity found in real aircraft constructions (curved panels, composite trim, possibility of a multilayer sound package, added constrained layer damping, isolating mounts, etc.). However, it represents a simple and realistic case study for the proposed models comparison.

Fig. 2 presents a schematic of the studied problem. It represents an acoustical plane wave P_{inc} impinging on the source side (panel 1) of the double wall assembly. The incident wave makes an angle θ with the y-axis and its projection in the xz plane makes an angle φ with the z axis. Its amplitude is P_0 and its wavenumber k_{air} can be decomposed in the x, y and z directions:

$$P_{\mathrm{inc}} = P_0 \exp[-\mathrm{j}k_x x - \mathrm{j}k_{y,\mathrm{air}} y - \mathrm{j}k_z z], \tag{1}$$

where

$$k_x = \omega/c_{\mathrm{air}} \sin\theta \sin\varphi, \tag{2}$$

$$k_{y,\mathrm{air}} = \frac{\omega}{c_{\mathrm{air}}} \cos\theta, \tag{3}$$

$$k_z = \frac{\omega}{c_{\mathrm{air}}} \sin\theta \cos\varphi. \tag{4}$$

The time dependence factor $\exp(\mathrm{j}\omega t)$ was omitted in Eq. (1) and will be considered implicit henceforth. Air with density ρ_{air} ($1.21\,\mathrm{kg\,m^{-3}}$) is present on both sides of the partition and the associated speed of sound is c_{air} ($342\,\mathrm{m\,s^{-1}}$). The effective density of the fiberglass filling the cavity is ρ_{cav} and the effective speed of sound and wavenumber in that fiber are, respectively, c_{cav} and k_{cav} ($k_{\mathrm{cav}} = \omega/c_{\mathrm{cav}}$). Note that by using an equivalent fluid approach for the fiberglass, ρ_{cav}, c_{cav} and k_{cav} are complex and frequency dependent [17]. When the incident wave hits the partition, a reflected wave P_r is created in the source region and a wave P_{tr} is transmitted into the receiver side. Inside the cavity, the pressure is P_{cav}. The two panels, whose displacements are noted W_1 and W_2 and velocities v_1 and v_2, respectively, have thicknesses e_1 and e_2 of 1 (first panel, source side) and 2 mm (second panel, receiving side). They both have Young modulus's E_1 and E_2 of $70 \times 10^9\,\mathrm{N\,m^{-2}}$, Poisson's ratios ν_1 and ν_2 of 0.33, internal damping ratios $\eta_{\mathrm{int},1}$ and $\eta_{\mathrm{int},2}$ of 1% and densities ρ_1 and ρ_2 of $2742\,\mathrm{kg\,m^{-3}}$. With these parameters, it is possible to calculate the mass per unit area m''_i, the bending stiffness D_i, the impedance $Z_{p.i}$ and the critical frequency $f_{\mathrm{cr},i}$ of the i'th panel [5]:

$$m''_i = \rho_i e_i, \tag{5}$$

$$D_i = \frac{E_i e_i^3 (1 + \mathrm{j}\eta_{\mathrm{int},i})}{12(1 - \nu_i^2)}, \tag{6}$$

$$Z_{p,i} = \mathrm{j}\omega m_i'' \left[1 - \frac{D_i k_x^4}{m_i'' \omega^2}\right], \tag{7}$$

$$f_{\mathrm{cr},i} = \frac{c_{\mathrm{air}}^2}{2\pi}\sqrt{\frac{m_i''}{D_i}} = \frac{\omega_{\mathrm{cr},i}}{2\pi}. \tag{8}$$

With the presented values, the critical frequencies are therefore around 12 kHz for the 1 mm panel and around 6 kHz for the 2 mm panel. Accordingly, a dip is expected in the transmission loss curve around 6 kHz. In practice, these dips are, however, highly sensitive to cavity and edge damping. The critical frequency of the 1 mm panel will not be captured in the presented study since TL measurements were taken in $\frac{1}{12}$ octave bands from 100 Hz to 10 kHz for both configurations (coupled and uncoupled). During the experiments, the edges of the wall were clamped on the mounting frame with wooden bars. To reduce the structural leaks to their minimum, neoprene was inserted between the two parts of that frame (receiving and source sides) all along the perimeter.

Finally, it is worth mentioning that for modeling purposes, the connecting channels will be considered transparent to the acoustic waves in the cavity; meaning the effects of lateral resonances in the cavity will be disregarded (cavity is not partitioned). In future work, it will be important to investigate this aspect of the problem; but at the present stage, it is not necessary since none of the studied models addresses this issue.

3. Decoupled approaches

3.1. Methodology

This section explains the simplified modeling methodology used in the decoupled approaches. On the source side of the double panel, an incident plane wave with acoustic power Π_{in} induces motion of the first panel. This motion creates a pressure inside the cavity and drives the structural bridges connecting the panels. Energy can therefore travel from the first panel to the second via two separate paths: the fluid-borne path through the cavity (energy transmission coefficient τ_C) and the structure-borne path through the bridges (energy transmission coefficient τ_B). The fundamental assumption of decoupled approaches is that these paths are independent and additive. Hence, the acoustic power emitted by the second panel Π_{out} corresponds to the power radiated by the panel due to the action of bridges Π_B plus the power radiated due to the action of the cavity pressure Π_C. The total transmission loss of the system $\mathrm{TL}_{\mathrm{tot}}$ can thus be written:

$$\mathrm{TL}_{\mathrm{tot}} = -10\log\left[\frac{\Pi_{\mathrm{out}}}{\Pi_{\mathrm{in}}}\right] = -10\log\left[\frac{\Pi_C + \Pi_B}{\Pi_{\mathrm{in}}}\right] = -10\log[\tau_C + \tau_B]. \tag{9}$$

At low frequencies, fluid-borne transmission is generally dominant and the bridged partition behaves similarly to the uncoupled one. However, at mid and high frequencies, the structural path prevails and reduces the TL considerably. The transition frequency between these two regimes is called the bridge frequency f_B and corresponds to the point when Π_B reaches Π_C.

In the following section, a calculation procedure for the fluid-borne transmission in the absence of bridges will be detailed. During the presented numerical simulations, this procedure will be common to all decoupled approaches even though the original authors of these approaches have presented their own view on this path. Attention will, therefore, be concentrated on structure-borne sound transmission formulations. This will render comparison easier between models by eliminating sources of discrepancy. Besides, it should not have a significant impact at mid and high frequencies since the structural path is dominant.

3.2. Fluid-borne transmission

When the line junctions are absent and the panels are modeled by thin infinite plates in bending, the analysis reduces to a 2D pattern in which $\varphi = \pi/2$. Using the transfer matrix method (TMM) [19], the pressures and

velocities at the forward and backward faces of the double wall system are related by:

$$\begin{bmatrix} P_1 \\ v_1 \end{bmatrix} = \mathbf{T} \begin{bmatrix} P_{\mathrm{tr}} \\ v_2 \end{bmatrix} = \begin{bmatrix} T_{11} & T_{12} \\ T_{21} & T_{22} \end{bmatrix} \begin{bmatrix} P_{\mathrm{tr}} \\ v_2 \end{bmatrix}, \tag{10}$$

where

$$\mathbf{T} = \begin{bmatrix} 1 & Z_{p,1} \\ 0 & 1 \end{bmatrix} \begin{bmatrix} \cos(k_{y,\mathrm{cav}}H) & \mathrm{j}\dfrac{\omega\rho_{\mathrm{cav}}}{k_{y,\mathrm{cav}}} \sin(k_{y,\mathrm{cav}}H) \\ \mathrm{j}\dfrac{k_{y,\mathrm{cav}}}{\omega\rho_{\mathrm{cav}}} \sin(k_{y,\mathrm{cav}}H) & \cos(k_{y,\mathrm{cav}}H) \end{bmatrix} \begin{bmatrix} 1 & Z_{p,2} \\ 0 & 1 \end{bmatrix}, \tag{11}$$

$$P_1 = P_{\mathrm{inc}} + P_r \text{ is the pressure on the receiving plate,} \tag{12}$$

$$k_{y,\mathrm{cav}} = \sqrt{k_{\mathrm{cav}}^2 - k_x^2} \text{ is the acoustic wavenumber inside the cavity.} \tag{13}$$

Making use of the global transfer matrix $\mathbf{T}$, the fluid-borne transmissibility $\tau_C(\theta)$ at a given angle θ is given by

$$\tau_C(\theta) = \left|\frac{P_{\mathrm{tr}}}{P_{\mathrm{inc}}}\right|^2 = \left|\frac{1+R}{T_{11} + T_{12}/Z_{\mathrm{ac}}}\right|^2, \tag{14}$$

where

$$R = \frac{P_r}{P_{\mathrm{inc}}} = \frac{Z - Z_{\mathrm{ac}}}{Z + Z_{\mathrm{ac}}}, \tag{15}$$

$$Z = \frac{P_1}{v_1} = \frac{T_{11}Z_{\mathrm{ac}} + T_{12}}{T_{21}Z_{\mathrm{ac}} + T_{22}}, \tag{16}$$

$$Z_{\mathrm{ac}} = \frac{P_{\mathrm{tr}}}{v_2} = \frac{\rho_{\mathrm{air}}c_{\mathrm{air}}}{\cos\theta}. \tag{17}$$

The diffuse field transmissibility $\bar{\tau}_C$ can be obtained by integrating over θ with the appropriate weighting [5]:

$$\bar{\tau}_C = \int_0^{\theta_{\mathrm{lim}}} \tau_C(\theta) \sin\theta \cos\theta \, \mathrm{d}\theta \Big/ \int_0^{\theta_{\mathrm{lim}}} \sin\theta \cos\theta \, \mathrm{d}\theta, \tag{18}$$

where $\theta_{\mathrm{lim}} = 90^\circ$ for random incidence and $\theta_{\mathrm{lim}} \approx 78^\circ$ for field incidence transmission.

3.3. Structure-borne transmission models

3.3.1. Sharp

In Refs. [2,3], Sharp formulated the problem of sound transmission through a double wall by using a decoupled approach. In his handling of the structure-borne path, he began by rewriting Eq. (9):

$$\mathrm{TL}_{\mathrm{tot}} = -10\log\left[\frac{\Pi_C + \Pi_B}{\Pi_{\mathrm{in}}}\right] = \mathrm{TL}_C - 10\log\left[1 + \frac{\Pi_B}{\Pi_C}\right], \tag{19}$$

where TL_C is the transmission loss of the isolated partition. For Π_C, he employed the expression of the power radiated by an infinite plate exposed to a sound field at normal incidence ($\theta = 0$):

$$\Pi_C \approx \rho_{\mathrm{air}}c_{\mathrm{air}}Sv_2^2, \tag{20}$$

where S is the area of the panel. For the near field radiation of sound bridges, he relied on Heckl's theory [20]:

$$\Pi_B \approx \rho_{\mathrm{air}}c_{\mathrm{air}}\kappa v_B^2, \tag{21}$$

where v_B is the rms velocity of the area κ over which the force induced in the second panel by the sound bridge is acting. For a line force, which is the studied case,

$$\kappa = \frac{2L_{\text{line}}\lambda_{\text{cr},2}}{\pi}, \tag{22}$$

where $\lambda_{\text{cr},2}$ is the critical wavelength of the second panel and L_{line} is the length of the line connection. In the present situation, L_{line} corresponds to the height of the wall L_z. If there are q equally spaced line junctions between the panels, $S = q \cdot L \cdot L_z$ and

$$\frac{\Pi_B}{\Pi_C} = \frac{2qL_z\lambda_{\text{cr},2}}{\pi S}\left(\frac{v_B}{v_2}\right)^2 = \frac{2c_{\text{air}}}{\pi L f_{\text{cr},2}}\left(\frac{v_B}{v_1}\right)^2\left(\frac{v_1}{v_2}\right)^2. \tag{23}$$

Sharp assumed that the velocity of the first panel was unaffected by the introduction of the line connection. Thereby, the ratio v_1/v_2 in Eq. (23) corresponds to the velocity ratio of the panels in the absence of bridges (v_1 and v_2 are the panel velocities). For frequencies below critical frequencies of both panels, he reduced this ratio to the following expression by making few simplifications:

$$\left(\frac{v_1}{v_2}\right)^2 = \begin{cases} \left(\dfrac{\omega^2 m_2'' H}{1.8\rho_{\text{air}}c_{\text{air}}^2}\right)^2, & f_{\text{mam}} < f < f_l, \\ \left(\dfrac{\omega m_2''}{1.8\rho_{\text{air}}c_{\text{air}}}\right)^2, & f > f_l, \end{cases} \tag{24}$$

$$f_l = \frac{c_{\text{air}}}{2\pi H}, \tag{25}$$

where

$$f_{\text{mam}} = \frac{1}{2\pi}\sqrt{\frac{1.8\rho_{\text{air}}c_{\text{air}}^2}{H}\left(\frac{m_1'' + m_2''}{m_1'' m_2''}\right)} \quad \text{is the mass}-\text{air}-\text{mass frequency [2].} \tag{26}$$

In Eq. (26), the factor 1.8 was introduced to account for the finite dimensions of the panels. Besides being limited to frequencies below the critical frequencies of both panels, the above formula was also developed by assuming air was present inside and outside the cavity. Thus, for the purpose of the problem addressed in this paper, a less restrictive expression will be employed by substituting Eq. (10) into Eq. (23) with $\theta = 0$:

$$\frac{v_1}{v_2} = Z_{\text{ac}}T_{21} + T_{22} = \cos(k_{\text{cav}}H) + \text{j}\,\sin(k_{\text{cav}}H)\left[\frac{Z_{p,2} + \rho_{\text{air}}c_{\text{air}}}{\rho_{\text{cav}}c_{\text{cav}}}\right]. \tag{27}$$

Sharp also assumed the connectors were rigid and massless. Combining this hypothesis with the analysis of the force induced in the bridge by the first panel, he showed that the ratio v_B/v_1 could be written:

$$\frac{v_B}{v_1} = \frac{Z_{\text{line},1}}{Z_{\text{line},1} + Z_{\text{line},2}}, \tag{28}$$

$$Z_{\text{line},i} = 2D_i^{1/4}\omega^{1/2}m_i''^{3/4}(1 + \text{j}), \tag{29}$$

where $Z_{\text{line},i}$ corresponds to the line impedance of the ith plate [5]. At that point, he combined Eqs. (19), (23), (24), (28) and (29), inserted values of air for the fluid inside and outside the cavity to reduce the TL formula to

its simplest expression. The obtained TL curve in the presence of line connections was parallel to the mass law above the bridge frequency f_B. Sharp also added a positive empirical correction of 5 dB to the curve after this point. The need for this correction was explained by the fact that assuming the response of the first panel is unaffected by the introduction of line connections is not accurate. In reality, the mass of the connectors and the impedance of the second panel exert a non-negligible influence that reduces the velocity of the panel. Yet, this correction will not be applied in this paper since it was intended to improve the modeling of panels bonded by connectors typically used in building constructions, i.e. wooden studs much heavier than the lightweight aluminum channels employed in the studied structure. Hence, Eq. (23) will be applied integrally except for the modified expression of the ratio v_1/v_2 (Eq. (27)).

3.3.2. Gu and Wang

To enhance the accuracy of predictions for double wall constructions linked with metallic channels showing a bending resilient character, Gu and Wang extended Sharp's theory by modeling the connection as a spring of equivalent translational stiffness K_t [4]. In the presence of flexible bridge connections, velocities v_{B1} and v_{B2} on each side of a bridge are not equal. Consequently, Eq. (23) was reformulated by inserting the ratio v_{B2}/v_{B1}:

$$\frac{\Pi_B}{\Pi_C}=\frac{2qL_z\lambda_{\mathrm{cr},2}}{\pi S}\left(\frac{v_{B2}}{v_2}\right)^2=\frac{2\lambda_{\mathrm{cr},2}}{\pi L}\left(\frac{v_{B1}}{v_1}\right)^2\left(\frac{v_{B2}}{v_{B1}}\right)^2\left(\frac{v_1}{v_2}\right)^2. \tag{30}$$

To evaluate this ratio, Gu and Wang regarded the problem as a classical mass–spring–mass system, where masses M_1 and M_2 are related to the effective masses of the panels (the mass of the connection was not considered). This leads to

$$\left(\frac{v_{B2}}{v_{B1}}\right)^2=\left(1-\omega^2\frac{M_2}{K_t}\right)^{-2}\approx\left(\frac{K_t}{\omega^2M_2}\right)^2 \quad \text{when} \quad \omega\gg\sqrt{\frac{K_t}{M_2}}. \tag{31}$$

Cremer and Heckl [21] showed that when a panel is excited by a line force and the length of the line is much larger than the width of the radiation area, the effective radiation area of the panel is approximately rectangular and its width is $\lambda_{\mathrm{air}}/2$. Accordingly, Gu and Wang proposed the following expression for M_2:

$$M_2=\frac{m_2''\lambda_{\mathrm{air}}L_z}{2}=\frac{\pi m_2''c_{\mathrm{air}}L_z}{\omega}. \tag{32}$$

Inserting Eq. (32) into Eq. (31), the following ratio v_{B2}/v_{B1} is obtained:

$$\left(\frac{v_{B2}}{v_{B1}}\right)^2=\left(\frac{K_t'}{\pi\omega m_2''c_{\mathrm{air}}}\right)^2, \tag{33}$$

where K_t' is the equivalent translational stiffness per unit length ($K_t'=K_t/L_z$) of the connector. For v_1/v_2, they used Sharp's formula while assuming $v_{B1}/v_1=1$. Then, they combined Eqs. (19), (24), (30) and (33) and inserted the values of air for the fluid inside and outside the cavity to calculate the transmission loss. However, they did not apply the 5 dB correction Sharp introduced to account for the modified response of the first panel.

To estimate K_t' for the current configuration, two approaches can be applied. First, if the bending character of the channels is considered, it can be assumed that the bending force F_B acts along the middle of the flange. Moreover, it can also be assumed that the major contribution to the deformation comes from the bending in the web of the channel. Knowing that the moment is equal to $F_BL_F/2$ in the web, the static translational stiffness per unit length is

$$K_t'=\frac{E_Be_B^3}{3HL_F^2}. \tag{34}$$

For the studied channels, $K_t'=22.8\times10^6\,\mathrm{N\,m^{-2}}$, which is in good agreement with the order of magnitude suggested in Ref. [4]. On the other hand, it would also be realistic to neglect the contribution of bending, because the added silicone layer should reduce the flange deformations and thus reduce the lever inducing bending in the web. In that case, the principal deformation would come from the axial deformation in the web

and the static translational stiffness per unit length becomes:

$$K'_t = \frac{E_B e_B}{H}, \tag{35}$$

which leads to a much stiffer value of $4.375 \times 10^9\,\mathrm{N\,m^{-2}}$. Since Gu and Wang's model was developed for flexible connectors, the estimation accounting for bending will be employed and the second estimation will be employed for other models. Yet, the outcome will still probably not be satisfactory, because the simplification Gu and Wang assumed for the ratio v_{B2}/v_{B1} at Eq. (31) will only be met above a few thousand hertz with the current parameters:

$$\omega \gg \sqrt{\frac{K_t}{M_2}} \Rightarrow f \gg \frac{K'_t}{2\pi^2 m''_2 c_{\mathrm{air}}} = 613\,\mathrm{Hz}. \tag{36}$$

This was to be expected since the model was developed for building wall types where the value of m''_2 is generally much higher. Finally, note that for the implementation of the Gu and Wang model, Sharp's expression for the ratio v_1/v_2 will once again be replaced by Eq. (27).

3.3.3. Fahy

The approach developed by Fahy is concurrently similar and different from Sharp's. As implicitly stated in the model of Sharp, Fahy assumed the dynamics of each stud independent of the others and their motion limited to the translation induced by incident bending waves normal to the stud-leaf connection lines. However, instead of using the ratio Π_B/Π_C to express the degradation of transmission loss caused by the presence of structural connections, he relied on the blocked pressure approximation to estimate directly the response of the first panel:

$$P_1 \approx 2P_{\mathrm{inc}} \approx Z_{p,1} v_1 \approx \mathrm{j}\omega m''_1 v_1 \quad \text{when} \quad f \ll f_{\mathrm{cr},1}. \tag{37}$$

This approximation inherently ignores the influence of the studs over the panel response and is also only valid when fluid loading effects are neglected. Assuming the panels identical ($Z_{\mathrm{line},1} = Z_{\mathrm{line},2} = Z_{\mathrm{line}}$) and taking the mass per unit length of the stud m'_B into account, Fahy expressed the stud (or bridge) velocity v_B induced by the first panel as follows:

$$v_B = \frac{Z_{\mathrm{line}} v_1}{2Z_{\mathrm{line}} + \mathrm{j}\omega m'_B}. \tag{38}$$

When m'_B is neglected and the line impedances of the two panels are different, this formula corresponds to Eq. (28) of Sharp's model. Finally, as Sharp did for Π_B, Fahy used the expression of the near field radiation power of a line force excited panel at frequencies below critical frequencies of panels [5]:

$$\Pi_B = \frac{\rho_{\mathrm{air}} |F_2|^2}{4(m'')^2 \omega} = \frac{\rho_{\mathrm{air}} |Z_{\mathrm{line},2} v_B|^2}{4(m'')^2 \omega} = \frac{\rho_{\mathrm{air}} |Z_{\mathrm{line}} v_B|^2}{4(m'')^2 \omega}, \tag{39}$$

where F_2 is the effective force per unit length applied by the stud on the second panel. Considering that there are q' connections per unit length ($q' = 1/L$) [5]:

$$\tau_B(\theta) = \frac{2q' \Pi_B \rho_{\mathrm{air}} c_{\mathrm{air}}}{|P_{\mathrm{inc}}|^2 \cos\theta}. \tag{40}$$

At that point, he inserted Eqs. (37)–(39) into (40) and neglected the impedance of the stud for practical building construction cases, to reduce $\tau_B(\theta)$ to

$$\tau_B(\theta) = \frac{2q' \rho_{\mathrm{air}}^2 c_{\mathrm{air}} c_l}{\sqrt{3}\omega^2 \rho_s^2 e \cos\theta}, \tag{41}$$

where ρ_s, c_l and e represent the density, quasi-longitudinal wave speed and thickness of the plate material, respectively. He also computed the ratio of this transmissibility to the one given by the oblique mass law part

of the fluid-borne path $\tau_{\text{mass-law}}(\theta)$:

$$\frac{\tau_B(\theta)}{\tau_{\text{mass-law}}(\theta)} = \frac{\tau_B(\theta)}{(\rho_{\text{air}} c_{\text{air}}/\omega m'' \cos\theta)^2} = \frac{2\cos\theta q' e c_l}{\sqrt{3} c_{\text{air}}} = \frac{0.7\cos\theta q' c_{\text{air}}}{f_{\text{cr}}}. \tag{42}$$

This expression is independent of frequency, indicating that the TL curve in the presence of line connections is parallel to the mass law as in Sharp's model.

In the presented results, the model of Fahy will be implemented integrally expect for Eq. (38) where different line impedances for the panels will be allowed. This means Eq. (41) will not be used. However, the mass of the connection will still be neglected even though it should not be so; for the studied case, at frequencies of interest (audio frequencies), the line impedances of the panels have a similar order of magnitude compared to the mass' impedance.

3.3.4. Davy

As Gu and Wang's model is an extension of Sharp's for flexible connectors, Davy [6,7] relied on Fahy's theory and allowed the bridge to depict a resilient character. He also allowed the panels to have different line impedances. Thereby, when the mechanical compliance per unit length $C'_M (C'_M = 1/K'_t)$ of the bridge is taken into account and half of the bridge mass m'_B is attributed to each panel (mass–spring–mass system), the velocity v_{B2} of the bridge on the side of the second panel is:

$$v_{B2} = \frac{Z_{\text{line},1} v_1}{Z_{\text{line},1} + [1 - (m'_B/2)C'_M\omega^2][Z_{\text{line},2} + j\omega m'_B] + j\omega C'_M Z_{\text{line},1} Z_{\text{line},2} - (m'_B/2)C'_M Z_{\text{line},1}\omega^2}. \tag{43}$$

Yet, the most interesting aspect of Davy's approach is the fact that he addressed the problem of resonant responses of the panels, thus allowing his model to be applied in the vicinity and above their critical frequencies. First, he used the fact that for each panel the energy ratio d_i of the resonant to the non-resonant forced (mass controlled) response is given by [22]

$$d_i = \frac{\pi\omega_{\text{cr},i}\sigma_i}{4\omega\eta_{\text{tot},i}}, \tag{44}$$

where σ_i represents the single sided radiation efficiency of the panel and $\eta_{\text{tot},i}$ its total loss factor. The latter is equal to the sum of the internal loss factor $\eta_{\text{int},i}$ and twice the single sided radiation loss factor $\eta_{\text{rad},i}$ ($\eta_{\text{tot},i} = 2\eta_{\text{rad},i} + \eta_{\text{int},i}$). The single sided radiation loss factor is related to the single sided radiation efficiency:

$$\eta_{\text{rad},i} = \frac{\rho_{\text{air}} c_{\text{air}}\sigma_i}{\omega m''_i}. \tag{45}$$

Next, Davy utilized the ratio r_i of the sound power radiated by the resonant vibration to the sound power radiated by the forced near field vibration of a line force on the ith panel [23]:

$$r_i = \frac{\sigma_i}{2\eta_{\text{tot},i}}\sqrt{\frac{\omega_{\text{cr},i}}{\omega}}. \tag{46}$$

The combined effect of the resonant response and radiation are summarized in the factor Q:

$$Q = (1 + d_{\text{low}})(1 + r_{\text{high}}), \tag{47}$$

where the subscript 'low' refers to the panel having the lowest critical frequency and the subscript 'high' to the panel having the highest critical frequency. This procedure was introduced to remove the apparent asymmetry. To compute σ, Davy relied on the corrected version of Maidanik's formulae given by Vér and Holmer [24]. For both plates, he limited the maximum value of σ to one to agree better with the sound transmission prediction of third octave band of noise.

Combining Eqs. (44)–(47) with (37), (39) and (40) and with (43) instead of (38), using the correction factor Q, integrating over θ (Eq. (18)) with $\theta_{\text{lim}} = \pi/2$ and neglecting m'_B in Eq. (43), Davy obtained the following

diffuse field transmission coefficient:

$$\bar{\tau}_B = \frac{64\rho_{\text{air}}^2 c_{\text{air}}^3 Q}{[g^2 + (4\omega^{1.5} m_1'' m_2'' c_{\text{air}} C_M' - g^2)^2] L\omega^2}, \tag{48}$$

$$g = m_1'' \sqrt{\omega_{\text{cr},2}} + m_2'' \sqrt{\omega_{\text{cr},1}}. \tag{49}$$

For the results of this paper, Davy's model will be implemented integrally except for the integration limit θ_{lim} that will be 78° instead of 90° (see Section 5.2). Thus, even though the mass impedance m_B' is not negligible in comparison to the line impedances of the panels (see Section 3.3.3), the latter is still neglected. For radiation efficiency calculations, the corrected version of Maidanik's formulae given by Vér and Holmer [24] will be employed and the dimensions of the sub-panels (1016 mm × 1220 mm) delimited by the channels adjacent to the line force will be used instead of the ones of the whole wall (2030 mm × 1220 mm). The maximum value of the radiation efficiency will be limited to one for both plates as Davy suggested.

4. Periodic approach

4.1. Derivation of the model

To provide a comprehensive periodic approach for the studied case, the reaction forces of the connectors applied to the panels in the x and z directions should be included which requires a refinement of the panels' model. Besides, geometrical features such as finite size of the wall and discrete screw fixing of the channels should also be considered. Due to this added complexity and given the scope of this study, the infinite thin plate in bending model will be conserved. Therefore, in addition to fluid loading, the panels are only subjected to forces per unit length $F_{1,n}$ and $F_{2,n}$ normal to the stud-leaf connection lines applied by the connectors at $x = nL$ and to moments per unit length $M_{1,n}$ and $M_{2,n}$ in the z direction. The two panels' equations of motion consequently take the following form:

$$[D_1\nabla^4 - \omega^2 m_1'']W_1 = P_{\text{inc}}||_{y=0} + P_r||_{y=0} - P_{\text{cav}}||_{y=0} - \sum_{n=-\infty}^{+\infty} F_{1,n}\delta(x-nL) + \frac{\partial}{\partial x}\left[\sum_{n=-\infty}^{+\infty} M_{1,n}\delta(x-nL)\right], \tag{50}$$

$$[D_2\nabla^4 - \omega^2 m_2'']W_2 = P_{\text{cav}}||_{y=H} - P_{\text{tr}}||_{y=H} - \sum_{n=-\infty}^{+\infty} F_{2,n}\delta(x-nL) + \frac{\partial}{\partial x}\left[\sum_{n=-\infty}^{+\infty} M_{2,n}\delta(x-nL)\right], \tag{51}$$

where $\nabla^4 = \partial^4/\partial x^4 + 2(\partial^4/\partial x^2\,\partial z^2) + \partial^4/\partial z^4$. To lighten the notation, let $\sum_n = \sum_{n=-\infty}^{+\infty}$. The response of the panels can be expressed as an infinite sum of "space-harmonics" [8,9,25]:

$$W_1 = \sum_n u_{1,n} \exp[-\mathrm{j}k_{x,n}x - \mathrm{j}k_z z], \tag{52}$$

$$W_2 = \sum_n u_{2,n} \exp[-\mathrm{j}k_{x,n}x - \mathrm{j}k_z z], \tag{53}$$

where

$$k_{x,n} = k_x + \frac{2n\pi}{L}. \tag{54}$$

Similarly, the pressures inside and outside the cavity can be represented by space-harmonic series [9]:

$$P_r = \sum_n \varepsilon_n \exp[-\mathrm{j}(k_{x,n}x - k_{y,\text{air},n}y + k_z z)], \tag{55}$$

$$P_{\text{cav}} = \sum_n \alpha_n \exp[-\mathrm{j}(k_{x,n}x + k_{y,\text{cav},n}y + k_z z)] + \beta_n \exp[-\mathrm{j}(k_{x,n}x - k_{y,\text{cav},n}y + k_z z)], \tag{56}$$

$$P_{\text{tr}} = \sum_n \xi_n \exp[-\mathrm{j}(k_{x,n}x + k_{y,\text{air},n}y + k_z z)], \tag{57}$$

where

$$k_{y,\mathrm{air},n} = \sqrt{k_{\mathrm{air}}^2 - k_{x,n}^2 - k_z^2}, \tag{58}$$

$$k_{y,\mathrm{cav},n} = \sqrt{k_{\mathrm{cav}}^2 - k_{x,n}^2 - k_z^2}. \tag{59}$$

Since the structure is periodic in the x direction, forces and moments both satisfy the periodicity relation [25]:

$$F_{i,n} = F_{i,0}\ \exp[-\mathrm{j}k_x nL], \tag{60}$$

$$M_{i,n} = M_{i,0}\ \exp[-\mathrm{j}k_x nL]. \tag{61}$$

In addition, Poisson's formula allows writing the sum of the δ functions as follows:

$$\sum_n \delta(x - nL) = \frac{1}{L}\sum_n \exp\left[\frac{-2\mathrm{j}n\pi x}{L}\right]. \tag{62}$$

Combining Eqs. (60), (61) and (62) yields:

$$\sum_n F_{i,n}\delta(x - nL) = \frac{F_{i,0}}{L}\exp[-\mathrm{j}k_x x]\sum_n \exp\left[\frac{-2\mathrm{j}n\pi x}{L}\right] = \frac{F_{i,0}}{L}\sum_n \exp[-\mathrm{j}k_{x,n}x], \tag{63}$$

$$\sum_n M_{i,n}\delta(x - nL) = \frac{M_{i,0}}{L}\exp[-\mathrm{j}k_x x]\sum_n \exp\left[\frac{-2\mathrm{j}n\pi x}{L}\right] = \frac{M_{i,0}}{L}\sum_n \exp[-\mathrm{j}k_{x,n}x]. \tag{64}$$

The factor $\exp[-\mathrm{j}k_x x]$ in the above equations corresponds to the phase factor introduced by Urusovskii in Ref. [12]. Finally, continuity conditions at fluid–panel interfaces require that

$$\left.\frac{\partial(P_{\mathrm{inc}} + P_r)}{\partial y}\right\|_{y=0} = \omega^2\rho_{\mathrm{air}}W_1, \tag{65}$$

$$\left.\frac{\partial P_{\mathrm{cav}}}{\partial y}\right\|_{y=0} = \omega^2\rho_{\mathrm{cav}}W_1, \tag{66}$$

$$\left.\frac{\partial P_{\mathrm{cav}}}{\partial y}\right\|_{y=H} = \omega^2\rho_{\mathrm{cav}}W_2, \tag{67}$$

$$\left.\frac{\partial P_{\mathrm{tr}}}{\partial y}\right\|_{y=H} = \omega^2\rho_{\mathrm{air}}W_2. \tag{68}$$

Substituting Eqs. (55)–(57) into Eqs. (65)–(68) and using the fact that the sums must be true for all values of x, the pressure coefficients and displacement amplitude coefficients are related for each n:

$$\varepsilon_n = P_0\delta_n - \frac{\mathrm{j}\omega^2\rho_{\mathrm{air}}u_{1,n}}{k_{y,\mathrm{air},n}}, \tag{69}$$

$$\alpha_n = \frac{\omega^2\rho_{\mathrm{cav}}\csc(k_{y,\mathrm{cav},n}H)}{2k_{y,\mathrm{cav},n}}(\exp[\mathrm{j}k_{y,\mathrm{cav},n}H]u_{1,n} - u_{2,n}), \tag{70}$$

$$\beta_n = \frac{\omega^2\rho_{\mathrm{cav}}\csc(k_{y,\mathrm{cav},n}H)}{2k_{y,\mathrm{cav},n}}(\exp[-\mathrm{j}k_{y,\mathrm{cav},n}H]u_{1,n} - u_{2,n}), \tag{71}$$

$$\xi_n = \frac{\mathrm{j}\omega^2\rho_{\mathrm{air}}\ \exp[\mathrm{j}k_{y,\mathrm{air},n}H]u_{2,n}}{k_{y,\mathrm{air},n}}, \tag{72}$$

where $\delta_0 = 1$ and $\delta_n = 0$ for $n \neq 0$. Inserting Eqs. (63), (64) and (69)–(72) into Eqs. (50) and (51) and requiring the sums to be true for all values of x, two coupled linear equations are obtained for each n:

$$\begin{bmatrix} A_{1,n} & \Delta_n \\ \Delta_n & A_{2,n} \end{bmatrix} \begin{bmatrix} u_{1,n} \\ u_{2,n} \end{bmatrix} = \begin{bmatrix} 2P_0\delta_n - \dfrac{F_{1,0}}{L} - \dfrac{\mathrm{j}k_{x,n}M_{1,0}}{L} \\ -\dfrac{F_{2,0}}{L} - \dfrac{\mathrm{j}k_{x,n}M_{2,0}}{L} \end{bmatrix}, \tag{73}$$

where

$$A_{1,n} = D_1(k_{x,n}^2 + k_z^2)^2 - m_1''\omega^2 + \frac{\mathrm{j}\omega^2\rho_{\mathrm{air}}}{k_{y,\mathrm{air},n}} + \frac{\omega^2\rho_{\mathrm{cav}}\,\cot(k_{y,\mathrm{cav},n}H)}{k_{y,\mathrm{cav},n}}, \tag{74}$$

$$A_{2,n} = D_2(k_{x,n}^2 + k_z^2)^2 - m_2''\omega^2 + \frac{\mathrm{j}\omega^2\rho_{\mathrm{air}}}{k_{y,\mathrm{air},n}} + \frac{\omega^2\rho_{\mathrm{cav}}\,\cot(k_{y,\mathrm{cav},n}H)}{k_{y,\mathrm{cav},n}}, \tag{75}$$

$$\Delta_n = -\frac{\omega^2\rho_{\mathrm{cav}}\,\csc(k_{y,\mathrm{cav},n}H)}{k_{y,\mathrm{cav},n}}. \tag{76}$$

By manipulating Eq. (73), explicit expressions of $u_{1,n}$ and $u_{2,n}$ are obtained:

$$u_{1,n} = \frac{1}{V_n}\left[2P_0A_{2,n}\delta_n - \frac{A_{2,n}(F_{1,0} + \mathrm{j}k_{x,n}M_{1,0})}{L} + \frac{\Delta_n(F_{2,0} + \mathrm{j}k_{x,n}M_{2,0})}{L}\right], \tag{77}$$

$$u_{2,n} = \frac{1}{V_n}\left[-2P_0\Delta_n\delta_n + \frac{\Delta_n(F_{1,0} + \mathrm{j}k_{x,n}M_{1,0})}{L} - \frac{A_{1,n}(F_{2,0} + \mathrm{j}k_{x,n}M_{2,0})}{L}\right], \tag{78}$$

where

$$V_n = A_{1,n}A_{2,n} - \Delta_n^2. \tag{79}$$

Summing Eqs. (77) and (78) over all n, a matrix system analogous to the one presented in Ref. [25] can be built:

$$\mathbf{W_0} = \begin{bmatrix} W_1 \\ \partial W_1/\partial x \\ W_2 \\ \partial W_2/\partial x \end{bmatrix}_{x=0} = \begin{bmatrix} S_{11} & S_{12} & S_{13} & S_{14} \\ S_{21} & S_{22} & S_{23} & S_{24} \\ S_{31} & S_{32} & S_{33} & S_{34} \\ S_{41} & S_{42} & S_{43} & S_{44} \end{bmatrix} \begin{bmatrix} F_{1,0} \\ M_{1,0} \\ F_{2,0} \\ M_{2,0} \end{bmatrix} + \frac{2P_0}{V_0} \begin{bmatrix} A_{2,0} \\ -\mathrm{j}k_{x,0}A_{2,0} \\ -\Delta_0 \\ \mathrm{j}k_{x,0}\Delta_0 \end{bmatrix} = \mathbf{SF_0} + \mathbf{P_0}, \tag{80}$$

where $\mathbf{W_0}$, $\mathbf{F_0}$ and $\mathbf{P_0}$ represent the displacement, force and excitation vectors, respectively. The coefficients S_{ij} of the $\mathbf{S}$ matrix are given by

$$\mathbf{S} = \frac{1}{L}\sum_n \frac{1}{V_n} \begin{bmatrix} -A_{2,n} & -\mathrm{j}k_{x,n}A_{2,n} & \Delta_n & \mathrm{j}k_{x,n}\Delta_n \\ \mathrm{j}k_{x,n}A_{2,n} & -k_{x,n}^2A_{2,n} & -\mathrm{j}k_{x,n}\Delta_n & k_{x,n}^2\Delta_n \\ \Delta_n & \mathrm{j}k_{x,n}\Delta_n & -A_{1,n} & -\mathrm{j}k_{x,n}A_{1,n} \\ -\mathrm{j}k_{x,n}\Delta_n & k_{x,n}^2\Delta_n & \mathrm{j}k_{x,n}A_{1,n} & -k_{x,n}^2A_{1,n} \end{bmatrix}. \tag{81}$$

To complete the solution, the reactions acting along the connection line at $x = 0$ have to be expressed in function of the panel displacements and slopes at that particular location. In the following sections, three coupling cases are described.

4.2. Coupling conditions

4.2.1. The general coupling case

A general coupling condition requires that the force and displacement vectors $\mathbf{F_0}$ and $\mathbf{W_0}$ are linked by a dynamic stiffness matrix $\mathbf{K}$:

$$\mathbf{F_0} = \begin{bmatrix} F_{1,0} \\ M_{1,0} \\ F_{2,0} \\ M_{2,0} \end{bmatrix} = \begin{bmatrix} K_{11} & K_{12} & K_{13} & K_{14} \\ K_{21} & K_{22} & K_{23} & K_{24} \\ K_{31} & K_{32} & K_{33} & K_{34} \\ K_{41} & K_{42} & K_{43} & K_{44} \end{bmatrix} \begin{bmatrix} W_1 \\ \partial W_1/\partial x \\ W_2 \\ \partial W_2/\partial x \end{bmatrix}_{x=0} = \mathbf{K}\mathbf{W_0}. \tag{82}$$

In this matrix, the terms K_{ij} are function of the inertial and resilient properties of the connectors. They can be found by modeling the links with lumped elements [11], by using FEM to account for more complex behavior (ex: presence of modes; complex geometry) or from experimental measurements. Once known, Eqs. (80) and (82) can be combined, leading to the following system of equations:

$$[\mathbf{I_4} - \mathbf{KS}]\mathbf{F_0} = \mathbf{K}\mathbf{P_0}, \tag{83}$$

where $\mathbf{I_4}$ is the 4×4 identity matrix. Having found forces $F_{i,0}$ and moments $M_{i,0}$, the latter can be substituted back into Eqs. (77) and (78) to find $u_{1,n}$ and $u_{2,n}$ for each n. The coefficients ξ_n of the transmitted pressure are then obtained through Eq. (72) and used to calculate the transmission coefficient $\tau_P(\theta,\varphi)$ of the periodic model [11]:

$$\tau_P(\theta,\varphi) = \frac{\sum_n |\xi_n|^2 \,\mathrm{Re}(k_{y,\mathrm{air},n})}{|P_0|^2 k_{y,\mathrm{air}}}. \tag{84}$$

At first sight, the implementation of this whole procedure may seem cumbersome, but instead of solving a $2 \times (2n+1)$ matrix system by replacing the expressions of reactions into Eq. (73), computations are reduced to sums and the resolution of a 4×4 system. The diffuse field transmission coefficient is finally calculated by integrating $\tau_P(\theta,\varphi)$ over θ and φ [5]:

$$\bar{\tau}_P = \frac{\int_0^{2\pi}\int_0^{\theta_{\lim}} \tau_P(\theta,\varphi)\,\sin\theta\,\cos\theta\,\mathrm{d}\theta\,\mathrm{d}\varphi}{\int_0^{2\pi}\int_0^{\theta_{\lim}} \sin\theta\,\cos\theta\,\mathrm{d}\theta\,\mathrm{d}\varphi} = \frac{2}{\pi}\frac{\int_0^{\pi/2}\int_0^{\theta_{\lim}} \tau_P(\theta,\varphi)\,\sin\theta\,\cos\theta\,\mathrm{d}\theta\,\mathrm{d}\varphi}{\int_0^{\theta_{\lim}} \sin\theta\,\cos\theta\,\mathrm{d}\theta\,\mathrm{d}\varphi}. \tag{85}$$

4.2.2. The mass–spring–mass approximation

To a first approximation, a mass–spring–mass system with constants independent of k_z and where forces are decoupled from slopes and moments decoupled from displacements can be used to model the connecting channels. In translation, the static stiffness K'_t (Eq. (35)) of the channels is employed and it is assumed half of the mass m'_B is located on each panel (lumped masses). In rotation, a similar scheme is also applied: the inertia term corresponds to I_O (see Table 2) and the static rotational stiffness per unit length K'_r corresponds to the bending rigidity per unit length of the channel web:

$$K'_r = \frac{E_B I'_z}{H} = \frac{E_B e_B^3}{12H}, \tag{86}$$

where I'_z is the second moment of area per unit length of the web with respect to the z axial axis. In the present case, $K'_r = 3.675 \times 10^3\,\mathrm{Nm\,rad^{-1}\,m^{-1}}$. The stiffness matrix $\mathbf{K}$ thus takes the following form:

$$\mathbf{K} = \begin{bmatrix} -0.5m'_B\omega^2 + K'_t & 0 & -K'_t & 0 \\ 0 & -0.5I_O\omega^2 + K'_r & 0 & -K'_r \\ -K'_t & 0 & -0.5m'_B\omega^2 + K'_t & 0 \\ 0 & -K'_r & 0 & -0.5I_O\omega^2 + K'_r \end{bmatrix}. \tag{87}$$

It is worth noting that with the current mass–spring–mass approximation in translation and rotation, the model presented here would be equivalent to the one developed in Ref. [11] if: (i) the cavity was empty (not filled with fiberglass), (ii) the rotational inertia was neglected and (iii) the integration was reduced to a 2D pattern in which $\varphi = \pi/2$.

In fact, even though the wavenumber k_z is absent in the rigidity matrix $\mathbf{K}$, the integration with respect to heading angle φ remains necessary since the propagation factors $k_{x,n}$ of the space harmonics vary with φ (see Eq. (54)). This means the TL will as well vary with φ even though the angle θ remains the same (this is similar to orthotropic behavior).

4.2.3. The beam-type coupling case

Another possibility is to assume the channels behave like beams stiffeners. In that case, continuity requires that

$$\mathbf{W_{1,0}} = \begin{bmatrix} W_1 \\ \partial W_1/\partial x \end{bmatrix}_{x=0} = \mathbf{W_{2,0}} = \begin{bmatrix} W_2 \\ \partial W_2/\partial x \end{bmatrix}_{x=0} = \mathbf{W_{B0}} = \begin{bmatrix} W_{B0} \\ \partial W_{B0}/\partial x \end{bmatrix}, \tag{88}$$

which implies from Eq. (80) that:

$$\mathbf{S_{11}F_{1,0}} + \mathbf{S_{12}F_{2,0}} + \mathbf{P_1} = \mathbf{S_{21}F_{1,0}} + \mathbf{S_{22}F_{2,0}} + \mathbf{P_2}, \tag{89}$$

where

$$\mathbf{S_{11}} = \begin{bmatrix} S_{11} & S_{12} \\ S_{21} & S_{22} \end{bmatrix}, \quad \mathbf{S_{12}} = \begin{bmatrix} S_{13} & S_{14} \\ S_{23} & S_{24} \end{bmatrix}, \quad \mathbf{S_{21}} = \begin{bmatrix} S_{31} & S_{32} \\ S_{41} & S_{42} \end{bmatrix}, \quad \mathbf{S_{22}} = \begin{bmatrix} S_{33} & S_{34} \\ S_{43} & S_{44} \end{bmatrix},$$
$$\mathbf{F_{1,0}} = \begin{bmatrix} F_{1,0} \\ M_{1,0} \end{bmatrix}, \quad \mathbf{F_{2,0}} = \begin{bmatrix} F_{2,0} \\ M_{2,0} \end{bmatrix}, \quad \mathbf{P_1} = \frac{2P_0}{V_0}\begin{bmatrix} A_{2,0} \\ -\mathrm{j}k_{x,0}A_{2,0} \end{bmatrix}, \quad \mathbf{P_2} = \frac{2P_0}{V_0}\begin{bmatrix} -\Delta_0 \\ \mathrm{j}k_{x,0}\Delta_0 \end{bmatrix}. \tag{90}$$

Defining $\mathbf{K_B}$ as the beam dynamic stiffness matrix and using properties of a general beam stiffener [26]:

$$\mathbf{F_{1,0}} + \mathbf{F_{2,0}} = \mathbf{K_B W_{B0}} = \begin{bmatrix} E_B I_x k_z^4 - m'_B\omega^2 & -c_x m'_B\omega^2 \\ -c_x m'_B\omega^2 & E_B \Gamma k_z^4 + G J_z k_z^2 - I_S\omega^2 \end{bmatrix}\begin{bmatrix} W_{B0} \\ \partial W_{B0}/\partial x \end{bmatrix}. \tag{91}$$

The constants in the matrix $\mathbf{K_B}$ are defined in Table 2. Combining Eqs. (88)–(91), the following 2×2 matrix systems are obtained and solved for $\mathbf{F_{1,0}}$ and $\mathbf{F_{2,0}}$:

$$[\mathbf{I_2} - \mathbf{K_B S_{11}} + (\mathbf{I_2} - \mathbf{K_B S_{12}})(\mathbf{S_{22}} - \mathbf{S_{12}})^{-1}(\mathbf{S_{11}} - \mathbf{S_{21}})]\mathbf{F_{1,0}} = \mathbf{K_B P_1} + (\mathbf{I_2} - \mathbf{K_B S_{12}})(\mathbf{S_{22}} - \mathbf{S_{12}})^{-1}(\mathbf{P_2} - \mathbf{P_1}), \tag{92}$$

$$[\mathbf{I_2} - \mathbf{K_B S_{12}} + (\mathbf{I_2} - \mathbf{K_B S_{11}})(\mathbf{S_{11}} - \mathbf{S_{21}})^{-1}(\mathbf{S_{22}} - \mathbf{S_{12}})]\mathbf{F_{2,0}} = \mathbf{K_B P_1} - (\mathbf{I_2} - \mathbf{K_B S_{11}})(\mathbf{S_{11}} - \mathbf{S_{21}})^{-1}(\mathbf{P_2} - \mathbf{P_1}), \tag{93}$$

where $\mathbf{I_2}$ is the 2×2 identity matrix. The procedure described in the general coupling case is then used to calculate the diffuse field transmission coefficient.

4.2.4. The special case of non-rigid and massless beam connections

When all the rigidity and the inertia of the connecting beams is neglected ($\mathbf{K_B} = \mathbf{0}$), reactions on both sides of the beam become equal and opposite and Eqs. (92) and (93) yield

$$\mathbf{F_{1,0}} = -\mathbf{F_{2,0}} = (\mathbf{S_{11}} + \mathbf{S_{22}} - \mathbf{S_{12}} - \mathbf{S_{21}})^{-1}(\mathbf{P_2} - \mathbf{P_1}). \tag{94}$$

5. Results

5.1. Experimental results

Fig. 3 presents the measured transmission loss of the uncoupled and coupled configurations (i.e. with and without line junctions). Predictions using the presented decoupled approaches are also shown together with

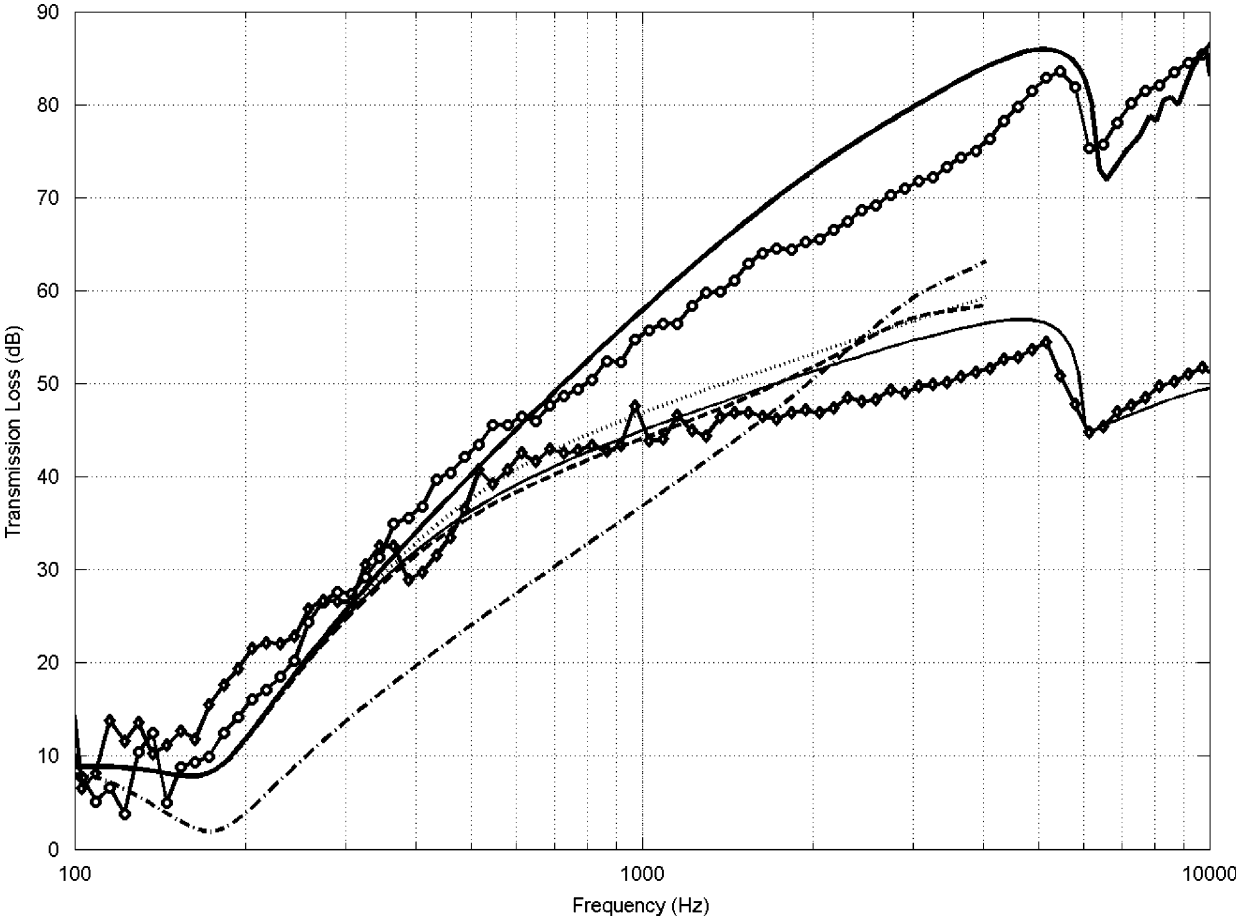

Fig. 3. Measured values vs. decoupled approaches. ◦: Measured values (no junctions); ◇: measured values (with junctions); —: no junctions (fluid-borne transmission only); — —: Sharp; · — · — · : Gu and Wang; ···: Fahy; —: Davy.

the prediction of the fluid-borne transmission path through the cavity (decoupled configuration). Comparing the two experimental curves, it is seen as expected that the structural path strongly reduces the TL at mid and high frequencies ($f > 300$ Hz). A dip associated to the critical frequency of the second panel (6 kHz) is observed in both curves. The coupled configuration also exhibits a dip around 400 Hz. Finally, at low frequencies ($f < 300$ Hz), the TL of the coupled configuration is higher. This is probably caused by the additional mass and/or stiffness provided by the junctions, even though that mass and rigidity is not distributed over the panels. However, results below 200 Hz should be discarded because of the volume limitation of the used transmission loss suite.

5.2. Decoupled approaches

The results of the comparison between the studied decoupled approaches and measurements are in Fig. 3. In the presented simulations, transmission loss is calculated in $\frac{1}{24}$ octave bands with a diffuse field integration limit θ_{lim} of 78°. Since the models of Sharp, Gu and Wang and Fahy cannot be applied above the critical frequency of either panel, they are plotted up to two-thirds of the critical frequency of the thicker panel. First, it is observed that overall the comparison between measurement and prediction for the fluid path (decoupled configuration) is satisfactory even though an overestimation is observed at mid to high frequencies. However, further investigation of the causes of this difference is not pursued since this is not important for the coupled configuration where the structure-borne transmission through the connectors is the dominant effect at these frequencies.

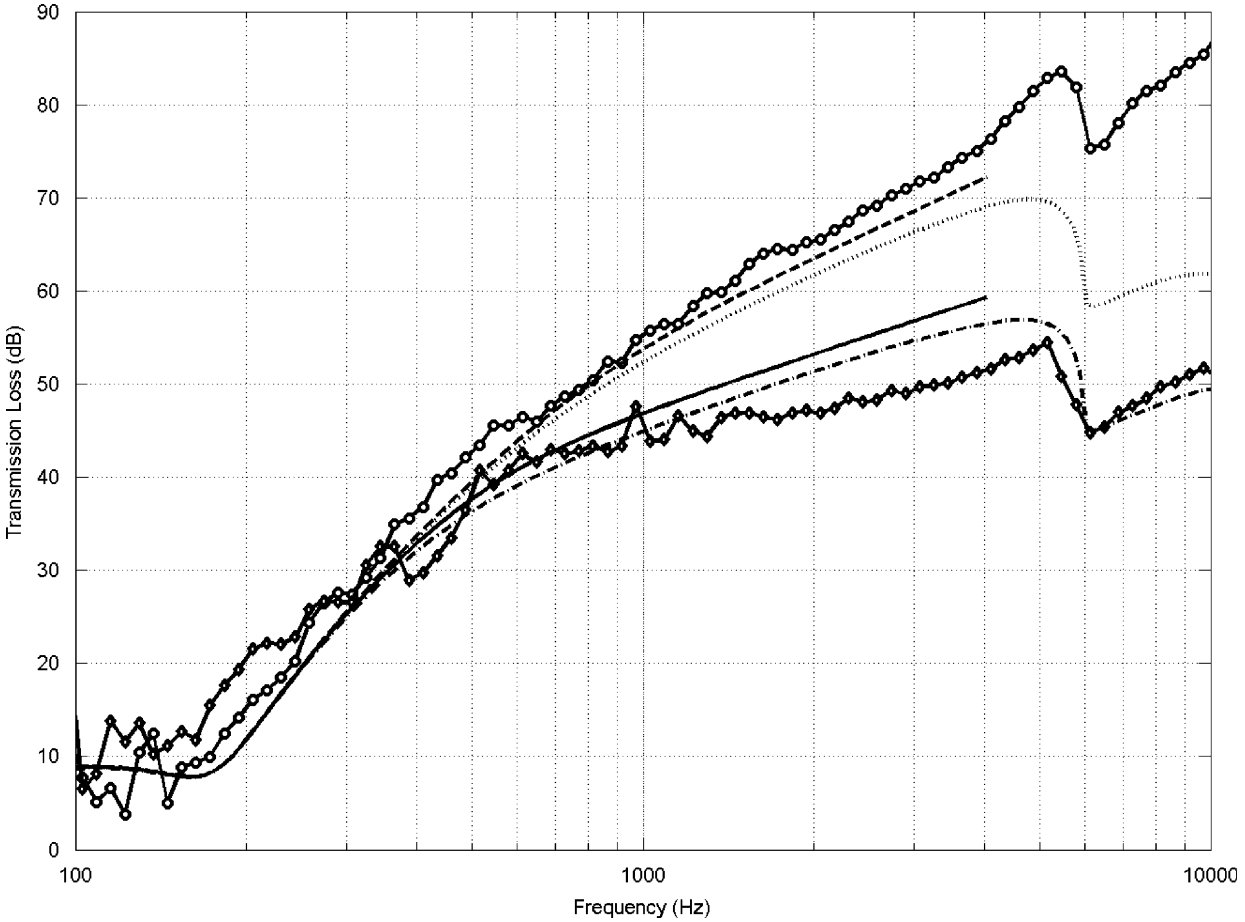

Fig. 4. Effect of mass on Fahy's and Davy's approaches. ◦: Measured values (no junctions); ◇: measured values (with junctions); —: Fahy, massless junctions (original); - - -: Fahy, junctions w/mass; ·—·—·: Davy, massless junctions (original); ···: Davy, junctions w/mass.

At first sight, the models of Sharp and Fahy appear fairly similar. Their prediction of the bridge frequency (f_B~300 Hz) is practically equal and in good agreement with both measurement and Davy's model. This is expected since equations in both models are similar except for the blocked pressure approximation in Fahy's approach. Above f_B, the growth rate of the two curves is 6 dB per octave as anticipated. The fact that Sharp's curve is not totally straight is due to the use of the modified expression for v_1/v_2. Above the bridge frequency and up to 2 kHz, the agreement with measurement is acceptable for Sharp and Fahy's models and good for Davy's model. In fact Davy's approach is good over the whole frequency range. Yet, this does not necessarily mean the physics of the problem is well reproduced. In fact, when the mass of the channels is not neglected in the models of Fahy and Davy, both approaches strongly overestimate the transmission loss as shown in Fig. 4. This reinforces the fact that the additional impedance of the channel mass should not be neglected in the presence of thin lightweight panels.

Finally, it is worth noting that Gu and Wang's model is off trend as projected (see Section 3.3.2), confirming its unsuitability for the current structure.

5.3. Periodic model

5.3.1. Convergence

Because the solution of the periodic model is expressed in series form, the number of terms n needs to be chosen to ensure convergence. The necessary number was determined at the highest frequency of interest

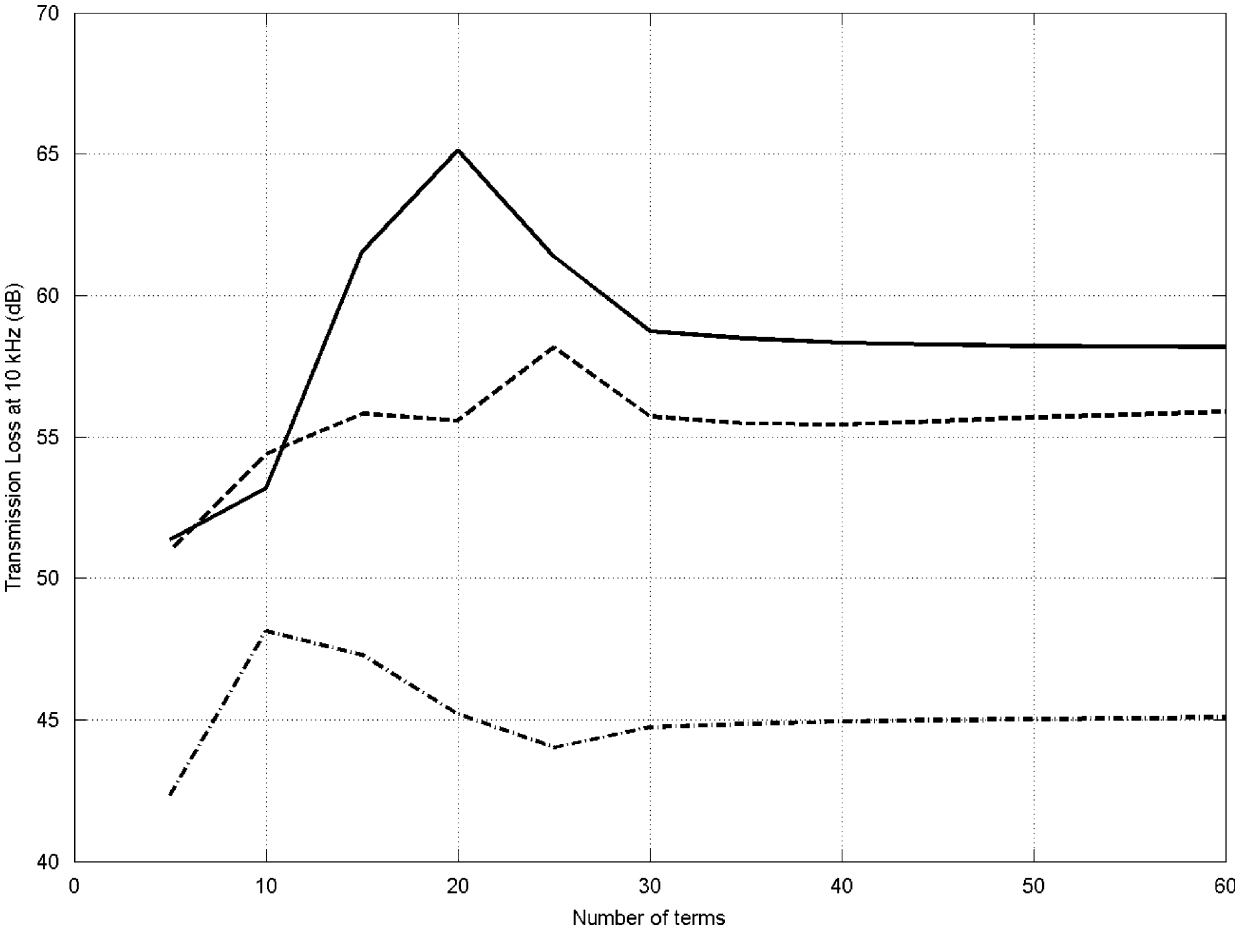

Fig. 5. Convergence of the periodic model. —: Mass–spring–mass case; - - -: beam case; ·—·—·: non-rigid and massless beam case.

(i.e. 10 kHz). Fig. 5 presents the diffuse field TL at 10 kHz as a function of n for the three coupling cases described in Section 4.2. At $n = 40$ ($n = -40$ to 40), it is observed that a satisfactory level of convergence has been reached.

5.3.2. Comparison with measurement

To study the performance of the periodic model, the predictions were made in $\frac{1}{24}$ octave bands and the results averaged over $\frac{1}{6}$ octave bands to smoothen the fluctuations in the TL curve caused by the pass/stop bands characteristic of periodic formulations. The integration limit θ_{lim} was again 78°. In Fig. 6, the results obtained for the three coupling cases described in Section 4.2 are shown. A fourth curve showing the results of the periodic model in the absence of connections is also presented. The latter was obtained using the mass–spring–mass coupling case in which the Young modulus E_B and the density ρ_B of the channels are artificially multiplied by a tiny factor equal to 10^{-9}. As expected, the result is equivalent to the fluid-borne transmission curve of Fig. 3.

At low frequencies ($f < 300$ Hz), the TL of the three coupled cases is higher compared to the uncoupled case. The periodic approach is thus able to account for the additional rigidity provided by the connecting channels. Yet, the agreement with measurements is not perfect. Around 400 Hz, the three cases capture well the dip observed in the experimental curve, meaning that the latter is probably caused by a pass band characteristic of the periodic structure [8–11,15,25]. Between 500 Hz and 2 kHz, the three periodic cases remain similar and in very good agreement with the experiment. However, above 2 kHz, the curve of the non-rigid and massless beam coupling case follows well measurements while the two others over predict it. Again and as in the case of

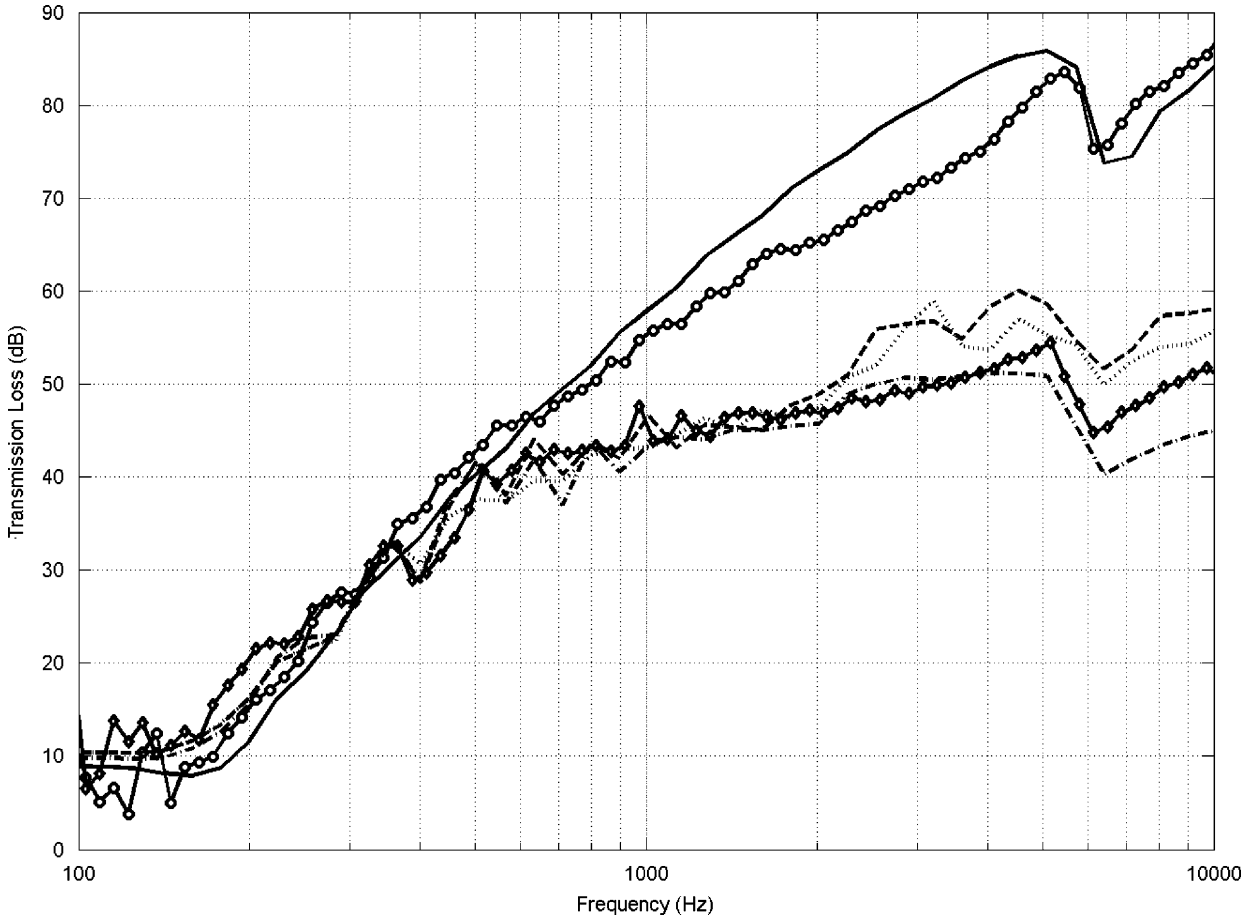

Fig. 6. Measured values vs. periodic model. ◦: Measured values (no junctions); ◇: measured values (with junctions); —: periodic model, no junctions; - - -: periodic model, mass–spring–mass case; ⋯: periodic model, beam case; · — · — ·: periodic model, non-rigid and massless beam case.

Davy's model, even if the prediction is excellent, the non-rigid and massless beam simplification is not realistic for thin lightweight panels.

On the other hand, the higher TL obtained with the mass–spring–mass formulation and the beam-type formulation indicates that the model needs refinement. By accounting for the resonant behavior of the walls, including a better assessment of the system damping, the accuracy of both cases could certainly be improved since the major differences occur in the vicinity of the critical frequency. Still, even with the observed discrepancies, the periodic approach is shown to be fairly well suited for the studied case in comparison with the predictions of the four studied decoupled approaches. The periodic model is able to reproduce the various subtleties of the physics of the problem with a small computational expense compared to methods such as FEM-BEM or hybrid FEM-SEA.

6. Conclusion

At the light of the obtained results, it is confirmed that the models of Sharp [2,3] and Fahy [5] were designed to provide a preliminary estimation on the effects of structural connections and not to describe the physics of all practical cases with an indisputable accuracy. Therefore, by integrating the resilient aspect of the connections, the models of Gu and Wang [4] and Davy [6,7] added a necessary degree of freedom to the problem even though Gu and Wang's formulation was found inadequate for the studied case.

The incorporation of the resonant response by Davy was also important to extend the range of applicability in the vicinity and above the critical frequency of the panels. The presented results corroborate Hongisto's conclusion that Davy's model remains the most comprehensive model of current decoupled approaches for bridged partitions. Yet, the fact that Davy's model does not include the mass reactance of junctions was shown to be arguable for the present structure, i.e. a structure where lightweight panels are employed as in aviation. However, for building constructions, this hypothesis is generally valid as discussed by Fahy [5].

In Ref. [27], Hongisto also suggested that a void still exists for a formulation that would do better than existing approaches: "According to the above conclusion, none of the existing double panel prediction models was applicable to all types of double wall structures. Therefore, a hybrid model should be developed as a combination of existing prediction models. This model should consider the surface mass, loss factor, lowest normal modes, critical frequency and dimensions of the wall. The cavity absorbent should be modeled by using its impedance and propagation factor, which is based either on measured data or derived data, e.g. on the basis of flow resistivity, dynamic stiffness and density." With the integration of the equivalent fluid model in the cavity in both decoupled and periodic models, that last condition was certainly fulfilled in this paper.

To add to Hongisto's recommendations, a complete formulation should also account for the modified response of the panel on the source side in the presence of connections. However, instead of applying a constant correction of 5 dB as Sharp did, the modifying factors should be a function of the properties of the connectors and the panels. Secondly, it would be ideal if coupling conditions could integrate both inertial and resilient effects of the connections. Finally, as in Davy's model, the range of applicability has to include frequencies in the vicinity and above critical frequencies of the panels.

The suggested strategy is therefore to keep appending complexity to the models based on the periodic assumption in order to improve the agreement with the experiments (finite dimensions of the wall, partitioning of the cavity by the connectors and discrete screw fixing between the panels and the connectors). In parallel, the periodic approaches will present an excellent benchmark for the improvement of existing decoupled approaches. Next, other attributes found in real aircraft constructions such as curvature, composite construction, added constrained layer damping, possibility of a multilayer sound package and isolating mounts should be included.

Acknowledgments

The authors wish to thank Maxime Bolduc, Patrick Levesque, Celse Kafui Amedin, Sébastien Ghinet and Simon Bastien for their technical assistance and help with the experiments.

References

[1] V. Hongisto, Sound insulation of double panels—comparison of existing prediction models, *Acta Acoustica* 92 (2006) 61–78.
[2] B.H. Sharp, A study of techniques to increase the sound insulation of building elements, Wyle Laboratories Report WR73-5, El Segundo, CA, USA, 1973.
[3] B.H. Sharp, Prediction methods for the sound transmission of building elements, *Noise Control Engineering Journal* 11 (1978) 53–63.
[4] Q. Gu, J. Wang, Effect of resilient connection on sound transmission loss of metal stud double panel partitions, *Chinese Journal of Acoustics* 2 (1983) 113–126.
[5] F. Fahy, P. Gardonio, *Sound and Structural Vibration*, second ed., Elsevier, Amsterdam, 2007.
[6] J.L. Davy, Predicting the sound insulation of stud walls, in: *Proceedings of Internoise 91*, vol. 1, Sydney, Australia, 1991, pp. 251–254.
[7] J.L. Davy, The sound transmission of cavity walls due to studs, in: *Proceedings of Internoise 93*, vol. 1, Leuven, Belgium, 1993, pp. 975–978.
[8] D.J. Mead, Free wave propagation in periodically supported infinite beams, *Journal of Sound and Vibration* 11 (2) (1970) 181–197.
[9] D.J. Mead, K.K. Pujara, Space-harmonic analysis of periodically supported beams: response to convected random loading, *Journal of Sound and Vibration* 14 (4) (1971) 525–541.
[10] J.-H. Lee, J. Kim, Analysis of sound transmission through periodically stiffened panels by space harmonic expansion method, *Journal of Sound and Vibration* 251 (2002) 346–366.
[11] J. Wang, T.J. Lu, J. Woodhouse, R.S. Langley, J. Evans, Sound transmission through lightweight double-leaf partitions: theoretical modeling, *Journal of sound and vibration* 286 (2005) 817–847.
[12] I.A. Urusovskii, Sound transmission through two periodically framed parallel plates, *Journal of Soviet Physics Acoustics* 38 (4) (1992) 411–413.

[13] G.-F. Lin, J.M. Garrelick, Sound transmission through two periodically framed parallel plates, *Journal of the Acoustical Society of America* 61 (1977) 1014–1018.
[14] D. Takahashi, Sound radiation from periodically connected harmonic double-plate structures, *Journal of Sound and Vibration* 90 (4) (1983) 541–557.
[15] B.R. Mace, The vibration of plates on two-dimensional periodic point supports, *Journal of Sound and Vibration* 192 (3) (1996) 629–643.
[16] R.J.M. Craik, R.S. Smith, Sound transmission through lightweight parallel plates—part II: structure-borne sound, *Applied Acoustics* 61 (2000) 247–269.
[17] J.F. Allard, *Propagation of Sound in Porous Media*, Elsevier Applied Science, 1993.
[18] W.D. Pilkey, *Formulas for Stress, Strain and Structural Matrices*, Second ed., Wiley, New York, 2005.
[19] Y. Hamada, H. Tachibana, Analysis of sound transmission loss of multiple structures by four-terminal network theory, in: *Proceedings of Internoise 85*, Munich, Germany, 1985, pp. 693–696.
[20] M. Heckl, Sound radiation from plates with point excitation, *Acustica* 9 (1959) 378.
[21] L. Cremer, M. Heckl, *Köperschall*, Springer, Berlin, 1967.
[22] M.J. Crocker, A.J. Price, Sound transmission using statistical energy analysis, *Journal of Sound and Vibration* 9 (3) (1969) 469–486.
[23] F. Fahy, *Sound and Structural Vibration*, First ed., Academic Press, London, 1985.
[24] I.L. Vér, C.I. Holmer, in: L.L. Beranek (Ed.), *Noise and Vibration Control*, McGraw-Hill, New York, 1971 (Chapter 11).
[25] B.R. Mace, Periodically stiffened fluid-loaded plates, I: response to convected harmonic pressure and free wave propagation, *Journal of Sound and Vibration* 73 (4) (1980) 473–486.
[26] M.J. Klaursbruckner, R.J. Pryputniewicz, Theoretical and experimental study of coupled vibrations of channel beams, *Journal of Sound and Vibration* 183 (2) (1995) 239–252.
[27] V. Hongisto, Airborne sound insulation of wall structures—measurement and prediction methods, Helsinki University of Technology, Laboratory of Acoustics and Audio Signal Processing, Report 56, Espoo, Finland, 2000.